Numerical modeling for different types of fractures

Xiaoqin (Jean) Cui, Laurence R. Lines and Edward S. Krebes

ABSTRACT

Research has shown that fractures can be modeled as a non-welded contact linear slip interface. Therefore, in the long wavelength limit, fractured homogeneous isotropic media are equivalent to transversely isotropic media (TI), and the azimuthal anisotropic parameters (Thomsen, 1986) are related to the fracture character parameters: tangential and normal compliances. Also, the elastic moduli of a fractured medium can be found by extending simple group theory calculation (Schoenberg and Muri, 1989) which is no longer used only for the non-welded contact linear slip interface. In this paper, seismic wave prorogation is affected by properties of the fractures in three different cases: horizontal, vertical and tilted fractures embedded in a homogeneous isotropic medium. We will discuss and illustrate the response to a fracture's width in the synthetic seismograms in each case later on.

INTRODUCTION

The upper crust of the earth is considerably layered with complex geometry interfaces between layers with different elastic parameters as well as a single layer medium with a unique elastic parameter. The two half spaces in the limit of the interface are either in perfectly welded contact in which the particle displacement and stresses are continuous across the interface, or there are imperfect non-welded contacts in which only the stresses are continuituous across the interface but the displacements are not. The imperfect non-welded contact interfaces are possibly formed due to artificial or natural compressions and unbalanced tension exerted on the medium, Thus there are non-unique patterns such as horizontal, vertical and tilted fractures. The non-welded contact interfaces are embedded in background media, and these types of the geological structures, are known as joints, fractures and faults, depending upon the length and the width of the interface. In other words, the width of the fracture does not necessarily approach zero. In general understanding, the non-welded contact interface separates geological formations into two side spaces, and forms an anisotropic media, in which fast and the slow shear waves propagate, that are orthogonally polarized to each other (Crampin, 1986). This phenomenon is known as shear wave splitting or birefringence. The fast shear wave is parallel and polarized to the direction of the fracture or maximum stress, whereas the slow shear wave is parallel to the direction of the minimum stress or perpendicular to the direction of the fracture. However, the width of the fracture is normally less than 10cm, so that it is difficult to detect the fracture structure with typical frequencies of the seismic waves (Lines et al, 2008). Regardless of the seismic resolution, it is still hard to indicate the fracture structure in a homogeneous isotropic medium because there is no impedance contrast around the fracture. In 1980, Schoenberg in his pioneering work produced a theory that a fracture is modeled as a non-welded contact linear slip interface, where the particle displacements are the discontinuous across interface and the stresses are continuituous across it. Additionally, the particle displacements are linearly proportional to the stresses. Pyrak-Nolte (1990) has confirmed non-welded contact interface theory by laboratory measurements.

Schoenberg and Muri (1989) presented the group theory formula based on the effective medium theory (Backus, 1962) to conveniently calculate the elastic moduli for the fractured and unfracture media. Nichols et al. (1989) and Hood (1991) show the solutions of the elastic moduli for a vertical fracture as a non-welded contact linear split interface vertically embedded in the background medium. Slawinski and Krebes (2002) simulated seismograms of SH and P-SV wave propagation in the non-welded contact linear slip interface (LS) by using 2D finite difference scheme.

As we know, the fracture structure strongly affects the permeability of the oil and gas reservoir, the width of the fracture H_f is a very important parameter for the recovery of the hydrocarbon reservoir exploration. The issues are presented in the first section of how to extend the elastic moduli formulations from the group theory calculation (Schoenberg and Muir, 1989) for the fractured medium where the linear fracture thickness H_i and relative thickness h_f have no value approaching to zero respect to the medium block thickness H (Figure 1). In the second section, to refer to the method of the generalized homogeneous finite difference forward scheme to simulate P-SV synthetic seismograms that recorded responses from the different fracture structure (Korn and Stockl, 1982. Slawinski and Krebes, 2002). Last but not least, we will discuss synthetic seismograms in which the propagating seismic waves hit the three types of the fractures including horizontal, vertical and tilted fractural structures embedded in a homogeneous background medium in the third section.

THE ELASTIC MODULI FOR FRACTURED MEDIA

Consider homogeneous media that are layered and perfectly bonded (Figure 1) to form the block layered medium. Let the block layered medium thickness, H, be smaller than minimum wavelength, and perpendicular to the vertical axis Z. It includes n constituent isotropic layers, i=1, 2…n. Respect to the block of the layered medium H, each thin constituent has an individual thickness H_i and a relative thickness $h_i=H_i/H$. Under the long wavelength assumption, once the thickness and impedance of a thin constituent approaches zero, the behavior of the layered medium blocks are the same as transverse isotropic medium, where homogeneous media combine with the non-welded contact linear slip interfaces paralleled to horizontal axis X (Schoenberg, 1980). In Hooke's law, the relationships of the stress σ_{ji}, elastic modulus c_{jk} and strain ε_{ki} for i-th constituent can be written as $\sigma_{ji} = \sum_{k=1}^{6} c_{jk}\varepsilon_{ki}$ $j=1\cdots6$; $i=1\cdots n$.

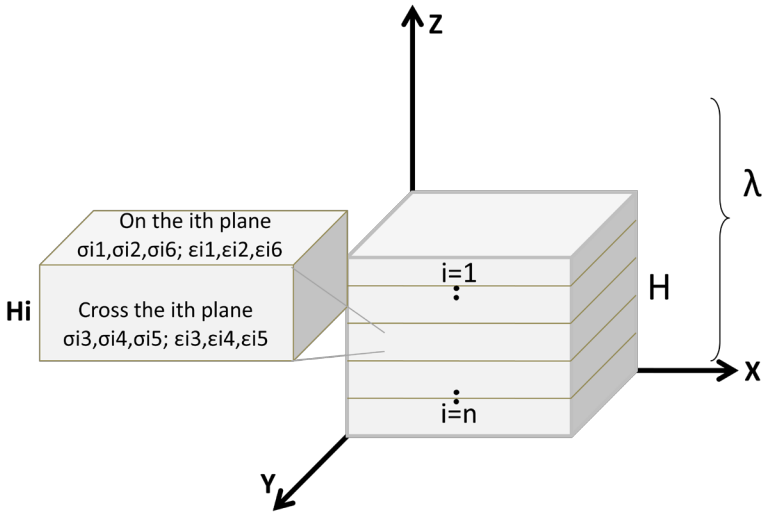

FIG. 1. The horizontal layered media include n constituents with thickness H_i. Each constituent have constant normal stresses and tangent stains but different tangent stresses and normal strains (discussed in detail in the text). The wavelength is much greater than the thickness of a constituent layer. Therefore, the block layered medium can be modeled as a particular type of transverse isotropic medium. This TI medium behavior is the same as a paralleled linear slip interface

The above the relationship of the stress and strain can be expressed as a matrix with an unconventional order of the elements

$$\begin{bmatrix}\sigma_1\\ \sigma_2\\ \sigma_6\\ \sigma_3\\ \sigma_4\\ \sigma_5\end{bmatrix}=\begin{bmatrix} \overbrace{\begin{matrix} c_{11} & c_{12} & 0\\ c_{21} & c_{22} & 0\\ 0 & 0 & c_{66}\end{matrix}}^{C_{TT}} & \overbrace{\begin{matrix} c_{13} & 0 & 0\\ c_{23} & 0 & 0\\ 0 & 0 & 0\end{matrix}}^{C_{TN}}\\ \underbrace{\begin{matrix} c_{31} & c_{32} & 0\\ 0 & 0 & 0\\ 0 & 0 & 0\end{matrix}}_{C'_{TN}} & \underbrace{\begin{matrix} c_{33} & 0 & 0\\ 0 & c_{44} & 0\\ 0 & 0 & c_{55}\end{matrix}}_{C_{NN}}\end{bmatrix}\begin{bmatrix}\varepsilon_1\\ \varepsilon_2\\ \varepsilon_6\\ \varepsilon_3\\ \varepsilon_4\\ \varepsilon_5\end{bmatrix} \qquad (1a)$$

The equation (1a) presents the relationship of stress and strain for the transverse isotropy medium with vertical symmetrical axis (VTI). The square with dash line divides the stiffness matrix c_{jk} into 4 stiffness sub-matrixes c_{TT}, c_{TN}, c_{NT} and c_{NN}. Where c_{NT} is the transpose of corresponding c_{TN} (Schoenberg and Muir, 1989). If the medium is a transverse isotropy with horizontal symmetrical axis (HTI), then equation (1a) can be reformat as HTI medium,

$$\begin{bmatrix}\sigma_2\\ \sigma_3\\ \sigma_4\\ \sigma_1\\ \sigma_5\\ \sigma_6\end{bmatrix}=\left[\begin{array}{ccc:ccc}c_{22} & c_{23} & 0 & c_{12} & 0 & 0\\ c_{23} & c_{33} & 0 & c_{13} & 0 & 0\\ 0 & 0 & c_{44} & 0 & 0 & 0\\ \hdashline c_{12} & c_{13} & 0 & c_{11} & 0 & 0\\ 0 & 0 & 0 & 0 & c_{55} & 0\\ 0 & 0 & 0 & 0 & 0 & c_{66}\end{array}\right]\begin{bmatrix}\varepsilon_2\\ \varepsilon_3\\ \varepsilon_4\\ \varepsilon_1\\ \varepsilon_5\\ \varepsilon_6\end{bmatrix} \quad (1b)$$

C_{TT}, C_{TN}, C'_{TN}, C_{NN}

The dashed line squares denote the VTI case. Following Backus's theory (1962), the layered medium are parallel to the horizontal axis x (Figure 1) and it assumed that all of the stress components acting on the paralleled to layering planes are the same in all layers in the media, i.e.,$\sigma_3 = \sigma_{33i}$, $\sigma_4 = \sigma_{23i}$, $\sigma_5 = \sigma_{13i}$. i=1⋯n. And all strain components acting in the plane of the layering are the same in all layers over thickness H, i.e. $\varepsilon_1 = \varepsilon_{11i}$, $\varepsilon_2 = \varepsilon_{22i}$, $\varepsilon_6 = 2\varepsilon_{12i}$. i=1⋯n. The other stress and strain components i.e. σ_1, σ_2, σ_6 and ε_3, ε_{24}, ε_5 are different from layer to layer, to calculate an average value will be taken to use as the constant value within a layer. Also the weighted average value of the thickness will be the value for the total value over full thickness H (Schoenberg and Muir, 1989).

$$\overline{\sigma_1} = \overline{\sigma_{11}} = \frac{1}{H}\sum_{i=1}^{n} h_i H\sigma_{1i}, \quad (2a)$$

$$\overline{\sigma_2} = \overline{\sigma_{22}} = \frac{1}{H}\sum_{i=1}^{n} h_i H\sigma_{2i}, \quad (2b)$$

$$\overline{\sigma_6} = \overline{\sigma_{12}} = \frac{1}{H}\sum_{i=1}^{n} h_i H\sigma_{6i}. \quad (2c)$$

And

$$\overline{\varepsilon_3} = \overline{\varepsilon_{33i}} = \frac{1}{H}\sum_{i=1}^{n} h_i H\varepsilon_{3i}, \quad (3a)$$

$$\overline{\varepsilon_4} = 2\overline{\varepsilon_{23i}} = \frac{1}{H}\sum_{i=1}^{n} h_i H\varepsilon_{4i}, \quad (3b)$$

$$\overline{\varepsilon_5} = 2\overline{\varepsilon_{13i}} = \frac{1}{H}\sum_{i=1}^{n} h_i H\varepsilon_{5i}. \quad (3c)$$

In the long wavelength limit, the normal strains can be written in terms of the individual layers strain as well as tangential stresses. So the vectors of the in-plane or tangential stresses and strains are

$$\overline{\sigma_T} = \begin{bmatrix}\overline{\sigma_1}\\ \overline{\sigma_2}\\ \overline{\sigma_6}\end{bmatrix},\ \varepsilon_T = \begin{bmatrix}\varepsilon_1\\ \varepsilon_2\\ \varepsilon_6\end{bmatrix} \text{ respectively.}$$

The vectors of the cross-plane or normal stresses and strains are

$$\sigma_N = \begin{bmatrix}\sigma_3\\ \sigma_4\\ \sigma_5\end{bmatrix},\ \overline{\varepsilon_N} = \begin{bmatrix}\overline{\varepsilon}_3\\ \overline{\varepsilon}_4\\ \overline{\varepsilon}_5\end{bmatrix} \text{ respectively.}$$

In the long-wavelength limit, the homogeneous medium moduli are found by taking the weighted average of the thickness. Therefore, the relationship of the stress and strain for the layered medium block (VTI) referring to equation (1a) will be

$$\overline{\sigma_T} = \overline{c_{TT}}\varepsilon_T + \overline{c_{TN}\varepsilon_N} \quad (4a)$$

$$\sigma_N = \overline{c_{NT}}\varepsilon_T + \overline{c_{NN}\varepsilon_N} \quad (4b)$$

Where c_{NT} is always the transpose of corresponding c_{TN}. Solve $\overline{\varepsilon_N}$ from the equation (4a) and substitute into the equation (4b). The resulting expressions are

$$\overline{\varepsilon_N} = \overline{c_{NN}^{-1}}\sigma_N - \overline{c_{NN}^{-1}c_{NT}}\varepsilon_T \quad (5a)$$

$$\overline{\sigma_T} = (\overline{c_{TT}} - \overline{c_{TN}c_{NN}^{-1}c_{NT}})\varepsilon_T + \overline{c_{TN}c_{NN}^{-1}}\sigma_N \quad (5b)$$

According to equations (3), equations (5) can be deduced to

$$\sum_{i=1}^{n} h_i\varepsilon_{Ni} = \sum_{i=1}^{n} h_i c_{NNi}^{-1}\sigma_N - (\sum_{i=1}^{n} h_i c_{NNi}^{-1} c_{TNi})\varepsilon_T$$

$$\sum_{i=1}^{n} h_i\sigma_{Ti} = (\sum_{i=1}^{n} h_i c_{TTi} - \sum_{i=1}^{n} h_i c_{TNi}\, c_{NNi}^{-1}c_{NTi})\varepsilon_T + \sum_{i=1}^{n} h_i c_{TNi}\, c_{NNi}^{-1}\sigma_N$$

Since $h_i = \frac{H_i}{H}$, so the normal strain and tangential stress for i^{th} constituent given

$$\overline{\varepsilon_{Ni}} = H_i c_{NNi}^{-1}\sigma_N - H_i c_{NNi}^{-1}c_{TNi}\varepsilon_T = g_i(3)\sigma_N - g_i(4)\varepsilon_T \quad (6a)$$

$$\overline{\sigma_{Ti}} = H_i c_{TNi}c_{NNi}^{-1}\sigma_N + H_i(c_{TTi} - c_{TNi}c_{NNi}^{-1}c_{NTi})\varepsilon_T = g_i(4)\sigma_N + g_i(5)\,\varepsilon_T \quad (6b)$$

Where $g(3)= H_i c_{NNi}^{-1}$, $g(4)= H_i c_{NNi}^{-1}c_{TNi}$ and $g(5)= H_i(c_{TTi} - c_{TNi}c_{NNi}^{-1}c_{NTi})$,called group matrix(Schoenberg and Muri, 1989). So the medium moduli c_{NN}, c_{TT}, c_{TN} and group matrix g(3), g(4), g(5) can transform into one another if $g(1)= H_i \neq 0$ and g(3) is invertible (Schoenberg and Muri, 1989).

$$\begin{bmatrix} c_{NNi} \\ c_{TNi} \\ c_{TTi} \end{bmatrix} = \begin{bmatrix} g_i(1)g_i^{-1}(3) \\ g_i(4)g_i^{-1}(3) \\ g_i(5) + g_i(4)g_i^{-1}(3)g_i^{t}(4)/g_i(1) \end{bmatrix} \quad (7)$$

It is clear that group theory offers formalism to the simple calculations for the elastic medium. It attempts to decompose the complex medium into a set of possible interleaved constituents, or equivalently, it enables us to form an equivalent medium from a sum of elements (Schoenberg and Muir, 1989).

Fractures + background medium ⟶ fractured medium

or, Fractures + background medium ⟵ fractured medium

In the long wavelength assumption, once the layered medium is deformed, such as the i^{th} constituent medium fractured, then the fracture layer will be soft, the cross-plane strain component $\overline{\varepsilon}_{Ni}$ will enlarge, while the in-plane strains ε_T relatively are decreased or are the same as the corresponding components in the background medium with constant value. As the i^{th} constituent its relative thickness, the limit of h_f approaches zero. In that case, equation (4b) is approximated to describe the relation of the stress and strain for a fracture, $\sigma_{Nf} \approx \overline{c_{NNf}}\,\overline{\varepsilon_{Nf}}$. It turns to that the fracture effects rely on modulus matrix c_{NNf}, which is related to on-plane stress and cross-plane strain of the fracture. There are the six

independent components but only 2 of the non-negative parameters in the matrix will describe the characters of the fracture if the fractured medium is a transversely isotopic medium (TI). Let $\overline{c_{NNf}^{-1}}=\mathbf{z}=\begin{bmatrix} z_N & 0 & 0 \\ 0 & z_T & 0 \\ 0 & 0 & z_T \end{bmatrix}$ for VTI medium. Here z_N and z_T are normal and tangential compliances of an average fracture of dimension length/stress (Schoenberg and Douma, 1988) respectively. Furthermore, the components of z in the plane of interface are equal. i.e. $c_{44} = c_{55}$.

If the width of the fracture does not approach zero and has nothing to infill the space, the fracture behavior will still exhibit linear action. Consider the width of the fracture layer as H_f, with the relative thickness as h_f respect to the medium thickness H, then $H_f = h_f H$. So the fracture layer moduli should be $c_{NNf} = h_f c_{NN}$, $c_{TNf} = h_f c_{TN}$, $c_{TTf} = h_f c_{TT}$, where c_{NN}, c_{TN}, and c_{TT} are elastic moduli of the media with thickness H. The group elements and modulus matrix are related:

$$\begin{bmatrix} g_f(1) \\ g_f(2) \\ g_f(3) \\ g_f(4) \\ g_f(5) \end{bmatrix} = \begin{bmatrix} h_f H \\ h_f^2 H\rho \\ H_f c_{NNf}^{-1} = H_f \frac{1}{h_f c_{NN}} \\ H_f c_{TNf} c_{NNf}^{-1} = H_f h_f c_{TN} \frac{1}{h_f c_{NN}} \\ H_f\left(c_{TTf} - c_{TNf} c_{NNf}^{-1}\right) = H_f\left(h_f c_{TT} - h_f c_{TN} \frac{1}{h_f c_{NN}} h_f c_{NT}\right) \end{bmatrix}$$

$$= \begin{bmatrix} h_f H \\ h_f^2 H\rho \\ H c_{NN}^{-1} \\ h_f H c_{TN} c_{NN}^{-1} \\ h_f^2 H(c_{TT} - c_{TN} c_{NN}^{-1} c_{NT} c_{NT}) \end{bmatrix} \qquad (9)$$

The equation (9) expresses the relationships of a group of elements and compliances for the nonzero width fracture. It is beneficial that the fractured medium compliances can be conveniently calculated through the simple adding and subtracting the group of elements (the equation 8), as well as for fractured medium stiffness calculation, it will be calculated by taking the inversion (equation 7). If the elastic moduli of the fractured transversely isotropic medium with vertical symmetric axis can be expressed as:

$$C^{VTI} = \begin{bmatrix} c_{11} & c_{12} & c_{13} & 0 & 0 & 0 \\ c_{21} & c_{22} & c_{23} & 0 & 0 & 0 \\ c_{31} & c_{32} & c_{33} & 0 & 0 & 0 \\ 0 & 0 & 0 & c_{44} & 0 & 0 \\ 0 & 0 & 0 & 0 & c_{55} & 0 \\ 0 & 0 & 0 & 0 & 0 & c_{66} \end{bmatrix} \qquad (10)$$

Where,

$$c_{11} = c_{22} = \left(1 + h_f^2\right)c_{11b} + \left[\frac{2h_f}{c_{33b}Z_N} - \left(1 + h_f^2\right)z_N\right]\frac{c_{13}^2}{1+c_{33}Zn_N}$$

$$c_{12} = c_{21} = \left(1 + h_f^2\right)c_{21b} + \left[\frac{2h_f}{c_{33b}Z_N} - \left(1 + h_f^2\right)z_N\right]\frac{c_{13b}^2}{1+c_{33b}Z_N}$$

$$c_{13} = c_{31} = c_{23} = c_{32} = \frac{c_{13b}(1+h_f)}{1+c_{33b}Z_N}$$

$$c_{33} = \frac{c_{33b}}{1+c_{33b}Z_N} \qquad c_{44} = \frac{c_{44b}}{1+c_{44b}Z_T} \qquad c_{55} = \frac{c_{55b}}{1+c_{55b}Z_T}$$

Considering Thomsen's parameters (1986), $\epsilon = \frac{c_{11}-c_{33}}{2c_{33}}$, $\gamma = \frac{c_{66}-c_{55}}{2c_{55}}$, Then,

$$E_N = \frac{2\epsilon - h_f^2}{(1+h_f^2)\left(1-\frac{c_{13b}^2}{c_{33b}^2}\right)+2h_f\frac{c_{13}^2}{c_{33b}^2}} \tag{11a}$$

$$E_T = 2\gamma \tag{11b}$$

Where $E_T = \mu z_T$, $E_N = (\lambda + 2\mu)z_N$ are non-negative dimensionless fracture compliance that express the ratio of compliance in the fractures to the corresponding compliance in unfracture medium. Therefore, in a homogeneous medium, such as shown in equation (11), the different width of the fracture has different fracture parameters z_N. The limit of $h_f \to 0$, will yield the elastic moduli for the transverse isotropic medium and this agrees with the solution from Schoenberg and Muir (1989) in which the fracture is modeled as a non-welded contact linear slip interface.

Cui and Lines (2011) presented a method in which the elastic moduli of the transverse isotropic with horizontal symmetric axis (HTI) can be solved from the transverse isotropic with vertical symmetric axis (VTI) by the coordinate's rotation. We used a similar method to give the elastic moduli of the transverse isotropic medium with horizontal symmetrical axis (1b). The similar formulation has been analogously applied to HTI medium. Thus any interface can be modeled since it can be deposed into the horizontal and vertical interfaces.

FINITE DIFFERENCE SCHEME OF P-SV WAVE PROPAGATING IN THE FRACTURE STRUCTURE

Several authors have studied seismic P-SV wave propagation in the fractured structure as a non-welded contact linear slip interface (LS). Chaisri and Krebes (2000) presented the reflection and transmission coefficients of PP and PS wave that passes through an imperfect non-welded contact interface in isotropic medium. Cui and Lines (2011) have studied the reflection and transmission coefficients of the elastic wave for the non-welded contact LS interface embedded in the VTI and HTI media. Coates and Schoenberg (1995) employed LS approach with equivalent medium theory to generate seismograms by employed finite difference method with staggered grid. Slawinski and Krebes (2002) extended the generalized homogeneous formulations (Korn and Stockl, 1982) to modeled fracture as LS by using finite difference scheme with adding the fictitious grid points. The generalized homogenous FD scheme takes more physical insights into account to the fracture forward modeling because the medium and boundary conditions (BCs) are imposed explicitly. The equation of motion governs the displacements outside the

discontinuity interface but non-welded contact boundary conditions are applied at the discontinuity interface. Definitely the fictitious points are introduced as the same points as the real grid on both side of the interface to make it possible to obtain BCs expressions for the displacement at the interface from either side of the medium. The BCs, $U^{z+}_{n+1/2} = U^{z-}_{n+1/2}$, where n+1/2 imply the interface at $z_{n+1/2}= (n+1/2)\Delta z$, the z^+ and z^-denote z-component displacements in the limit of the interface that approaches the upper edge and lower edge of the media (Figure 2), respectively. Figure 2 shows fictitious grid point at n+1 as $\tilde{U}_{n+1}$, belongs to the upper medium and similarly fictitious grid point at n as $\tilde{U}_n$, and belongs to lower medium. It is beneficial that fictitious points introduce the material discontinuity across the interface. It is assumed that the fracture as a non-welded the interface should be aligned with the grid boundary as $z_{n+1/2} = (n + 1/2)\Delta z$.

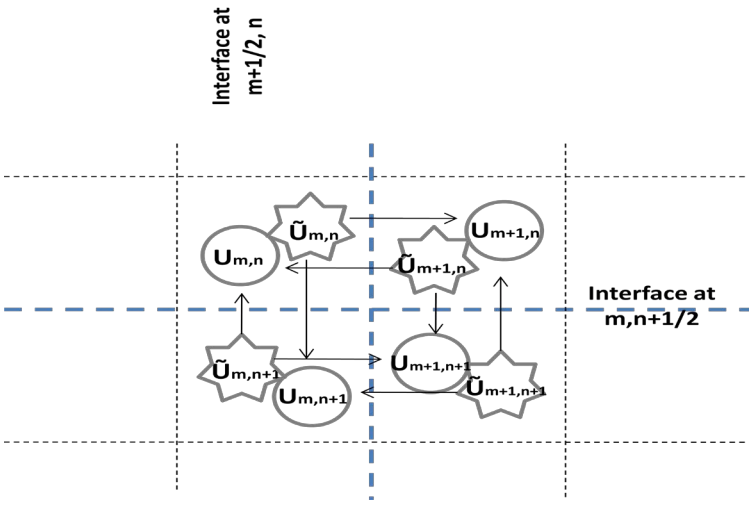

FIG. 2. The fictitious points and real points are in the same grid. Real points denoted by circles, fictitious points by flowers. Fictitious points below (left) the interface belong to upper (right) medium, and vice versa. Between every two neighboring points there exists an interface (blue dash lines)

From the equation of motion for a homogeneous isotropic medium, P-SV equation of motion for 2D such medium in xz -plane may be written as (Aki and Richards, 1980)

$$\frac{\partial^2 \mathbf{U}}{\partial^2 t} = \mathbf{A}\frac{\partial^2 \mathbf{U}}{\partial x^2} + \mathbf{B}\frac{\partial^2 \mathbf{U}}{\partial x\,\partial z} + \mathbf{C}\frac{\partial^2 \mathbf{U}}{\partial z^2} \qquad (13)$$

Where $\mathbf{U} = \begin{pmatrix} U^x \\ U^z \end{pmatrix}$, $\mathbf{A}=\begin{pmatrix} v_p^2 & 0 \\ 0 & v_s^2 \end{pmatrix}$, $\mathbf{B}=\begin{pmatrix} 0 & v_p^2 - v_s^2 \\ v_p^2 - v_s^2 & 0 \end{pmatrix}$, $\mathbf{C}=\begin{pmatrix} v_s^2 & 0 \\ 0 & v_p^2 \end{pmatrix}$. And v_p and v_s are pressure wave velocity and shear wave velocity, respectively. So the elastic wave of 2D finite difference scheme is

$$\mathbf{U}_{m,n}^{t+1}=-\mathbf{U}_{m,n}^{t-1}+2\mathbf{U}_{m,n}^{t}+\left(\frac{\Delta t}{\Delta x}\right)^2\mathbf{A}\left(\mathbf{U}_{m+1,n}^{t}-2\mathbf{U}_{m,n}^{t}+\mathbf{U}_{m-1,n}^{t}\right)$$
$$+\left(\frac{\Delta t^2}{\Delta x \Delta z}\right)\mathbf{B}\left(\mathbf{U}_{m+1,n+1}^{t}-\mathbf{U}_{m+1,n-1}^{t}-\mathbf{U}_{m-1,n+1}^{t}+\mathbf{U}_{m-1,n-1}^{t}\right)$$
$$+\left(\frac{\Delta t}{\Delta z}\right)^2\mathbf{C}\left(\mathbf{U}_{m,n+1}^{t}-2\mathbf{U}_{m,n}^{t}+\mathbf{U}_{m,n-1}^{t}\right) \quad (14)$$

Where, t denotes time, m and n are indicate grid number in the x and z directions, and $\Delta\mathbf{t}$, $\Delta\mathbf{x}$ and $\Delta\mathbf{z}$ are the time and space sizes, respectively. The finite difference scheme from the generalized homogeneous approach (Slawinski and Krebes, 2002) is (Figure 2)

$$\mathbf{U}_{m,n}^{t+1}=-\mathbf{U}_{m,n}^{t-1}+2\mathbf{U}_{m,n}^{t}+\left(\frac{\Delta t}{\Delta x}\right)^2\mathbf{A}\left(\widetilde{\mathbf{U}}_{m+1,n}^{t}-2\mathbf{U}_{m,n}^{t}+\widetilde{\mathbf{U}}_{m-1,n}^{t}\right)$$
$$+\left(\frac{\Delta t}{\Delta z}^2\right)\mathbf{C}\left(\widetilde{\mathbf{U}}_{m,n+1}^{t}-2\mathbf{U}_{m,n}^{t}+\widetilde{\mathbf{U}}_{m,n-1}^{t}\right) \quad (15)$$

The equation of motion (15) used the fictitious points to impose explicitly BCs at $z_{n+1/2}=(n+1/2)\Delta z$ for the interface that separate homogeneous isotropic medium into two half spaces.

In the linear slip approach (Schoenberg, 1980), only stresses are continuous across the interface, but displacements are not. All displacements are the linear function of the stresses i.e.

$$U^{x+}-U^{x-}=\eta_T\sigma^{zx+(-)} \quad (16a)$$
$$U^{z+}-U^{z-}=\eta_N\sigma^{zz+(-)} \quad (16b)$$
$$\sigma^{zx+(-)}=\sigma^{zx-(+)} \quad (16c)$$
$$\sigma^{zz+(-)}=\sigma^{zz-(+)} \quad (16d)$$

Where

$$\sigma^{zx}=\mu\left(\frac{\partial U^z}{\partial x}+\frac{\partial U^x}{\partial z}\right) \quad (16e)$$
$$\sigma^{zz}=\lambda\frac{\partial U^x}{\partial x}+(\lambda+2\mu)\frac{\partial U^z}{\partial z} \quad (16f)$$

Sign + and – express the upper and the lower media of the interface, respectively. Substituting equations (16e) and (16f) into (16a) and (16b), the difference in displacement of x- component at interface is:

$$U^{x+}-U^{x-}=\eta_T\mu(\partial_x U^z+\partial_z U^x) \quad (17a)$$
$$\eta_T(\mu(\partial_x U^z+\partial_z U^x))^+=\eta_T(\mu(\partial_x U^z+\partial_z U^x))^- \quad (17b)$$

The difference in displacement of z-component at interface is:

$$U^{z+} - U^{z-} = \eta_N(\lambda\,\partial_x U^x + (\lambda + 2\mu)\,\partial_z U^z) \tag{18a}$$

$$\eta_N(\lambda\,\partial_x U^x + (\lambda + 2\mu)\,\partial_z U^z)^+ = \eta_N(\lambda\,\partial_x U^x + (\lambda + 2\mu)\,\partial_z U^z)^- \tag{18b}$$

Using the central difference operator and the averaging operator with fictitious points to form a non-welded contact linear slip interface at $z_{n+1/2} = (n + 1/2)\Delta z$ embedded in the isotropic background medium,

$$\begin{aligned}\Delta U^x_{m,n+1/2} &= \frac{1}{2}(U^x_{m,n+1} + \tilde{U}^x_{m,n}) - \frac{1}{2}(\tilde{U}^x_{m,n+1} + U^x_{m,n}) \\ &= z_T\mu_{m,n+1}\left(\frac{U^z_{m+1,n+1} - U^z_{m-1,n+1}}{2\Delta x} + \frac{U^x_{m,n+1} - \tilde{U}^x_{m,n}}{\Delta z}\right) \\ &= z_T\mu_{m,n+1}\left(\frac{\partial U_z}{\partial x} + \frac{\partial U_x}{\partial z}\right)\end{aligned} \tag{19a}$$

$$\begin{aligned}\sigma^{xz}_{m,n+1} &= z_T\mu_{m,n+1}\left(\frac{U^z_{m+1,n+1} - U^z_{m-1,n+1}}{2\Delta x} + \frac{U^x_{m,n+1} - \tilde{U}^x_{m,n}}{\Delta z}\right) \\ &= z_T\mu_{m,n+1}\left(\frac{U^z_{m+1,n} - U^z_{m,n+1}}{2\Delta x} + \frac{\tilde{U}^x_{m,n+1} - \tilde{U}^x_{m,n}}{\Delta z}\right) = \sigma^{xz}_{m,n}\end{aligned} \tag{19b}$$

Where $\mu_{m,n} = \mu_{m,n+1} = \mu$, $\lambda_{m,n} = \lambda_{m,n+1} = \lambda$ are isotropic medium parameter. The compliances η_T and η_N are nonzero constants for all boundaries that exist between grid rectangles. So the fictitious points of x-component for z-normal boundary $\tilde{U}^x_{m,n}$ and $\tilde{U}^x_{m,n+1}$ can be solved from (19) since there are two equations with two unknown fictitious points. Compare the xz-components of stress BCs are in equation (17) and the zz-components stress BCs are in equation (18), it is explicit that the terms U_x, $\eta_T\mu\,\partial_x$, $\eta_T\mu\,\partial_z$ for the xz-component of stress BCs that are in equation (17) can be replaced by the terms U_z, $\eta_N\lambda\,\partial_x$, $\eta_N(\lambda + 2\mu)\,\partial_z$ respectively to form a zz-component stress BCs terms in equation (18). Therefore, it may easily solve z-component fictitious point $\tilde{U}^z_{m,n}$ and $\tilde{U}^z_{m,n+1}$ for z-normal boundary.

Let $\Delta x = \Delta z = h$, and define the dimensionless non-welded parameters $\delta = \frac{z_T\mu}{h}$, $\Upsilon = \frac{z_N\lambda}{h}$, $\emptyset = \frac{z_N(\lambda+2\mu)}{h}$, then the fictitious points for z-normal boundary are

$$\begin{aligned}\tilde{\mathbf{U}}_{m,n} &= \tilde{\mathbf{A}}(\mathbf{U}_{m,n} + \tilde{\mathbf{B}}\mathbf{U}_{m,n+1} - \frac{1}{4}\tilde{\mathbf{C}}(\mathbf{U}_{m+1,n} - \mathbf{U}_{m-1,n}) \\ &\quad + \frac{1}{4}\tilde{\mathbf{D}}(\mathbf{U}_{m+1,n+1} - \mathbf{U}_{m-1,n+1})\end{aligned} \tag{20a}$$

$$\begin{aligned}\tilde{\mathbf{U}}_{m,n+1} &= \tilde{\mathbf{A}}(\mathbf{U}_{m,n} + \tilde{\mathbf{B}}\mathbf{U}_{m,n+1} - \frac{1}{4}\tilde{\mathbf{D}}(\mathbf{U}_{m+1,n} - \mathbf{U}_{m-1,n}) \\ &\quad + \frac{1}{4}\tilde{\mathbf{C}}(\mathbf{U}_{m+1,n+1} - \mathbf{U}_{m-1,n+1})\end{aligned} \tag{20b}$$

Where $\mathbf{U}_{m,n} = \begin{bmatrix} U^x_{m,n} \\ U^z_{m,n} \end{bmatrix}$ $\tilde{\mathbf{A}} = \begin{bmatrix} \frac{1}{1+\delta} & 0 \\ 0 & \frac{1}{1+\emptyset} \end{bmatrix}$, $\tilde{\mathbf{B}} = \begin{bmatrix} \frac{\delta}{1+\delta} & 0 \\ 0 & \frac{\emptyset}{1+\emptyset} \end{bmatrix}$

$$\tilde{\mathbf{C}}=\begin{bmatrix} 0 & \frac{1+2\delta}{1+\delta} \\ \frac{\Upsilon(1+2\emptyset)}{\emptyset(1+\emptyset)} & 0 \end{bmatrix}, \quad \tilde{\mathbf{D}}=\begin{bmatrix} 0 & \frac{1}{1+\delta} \\ \frac{\Upsilon}{\emptyset(1+\emptyset)} & 0 \end{bmatrix}.$$

Equations (20) can be reformed to find the difference displacement between the fictitious and corresponding real grid points. This may be help to understand the geometry of the points (m,n) and (m,n+1) relative to boundary at n+1/2. If it takes interchange from U_x, m, Δx into U_z, n, Δz, then the x-normal component $\tilde{\mathbf{U}}_{m,n}$ $\tilde{\mathbf{U}}_{m+1,n}$ (Slawinski, 1999) can be solved by using fictitious points to express the boundary at m+1/2 between points (m,n) and (m+1,n) . Thus FD scheme of the P-SV propagation in the homogeneous medium with a non-welded contact linear slip interface should be

$$\mathbf{U}_{m,n}^{t+1} = -\mathbf{U}_{m,n}^{t-1} + 2\mathbf{U}_{m,n}^{t} + \frac{1}{\rho}\left(\frac{\Delta t}{h}\right)^2\left(\mathbf{F}\hat{\mathbf{N}}\mathbf{F}(\mathbf{U}_{m+1,n}^{t} - 2\mathbf{U}_{m,n}^{t} + \mathbf{U}_{m-1,n}^{t})\right.$$
$$+\hat{\mathbf{N}}(\mathbf{U}_{m,n+1}^{t} - 2\mathbf{U}_{m,n}^{t} + \mathbf{U}_{m,n-1}^{t})$$
$$\left.+\frac{1}{4}(\mathbf{F}\hat{\mathbf{G}}\mathbf{F} + \hat{\mathbf{G}})(\mathbf{U}_{m+1,n+1}^{t} - \mathbf{U}_{m+1,n-1}^{t} - \mathbf{U}_{m-1,n+1}^{t} + \mathbf{U}_{m-1,n-1}^{t})\right)$$

Where $\mathbf{F} = \begin{bmatrix} 0 & 1 \\ 1 & 0 \end{bmatrix}$, $\hat{\mathbf{N}} = \begin{bmatrix} \frac{\mu}{1+\delta} & 0 \\ 0 & \frac{\lambda+2\mu}{1+\emptyset} \end{bmatrix}$, $\hat{\mathbf{G}} = \begin{bmatrix} 0 & \frac{\mu}{1+\delta} \\ \frac{\lambda}{1+\emptyset} & 0 \end{bmatrix}$

SEISMOGRAMS AND DISCUSSIONS

We have implemented Matlab code to present numerical results to answer two questions: What are the physical effects of the three types of the fracture models being related to the non-welded contact linear interfaces embedded in the homogeneous isotropic medium? What is the physical response of synthetic seismogram with and without the width of the fracture?

For a better understanding of the fracture's properties, it is useful to investigate numerically PP and PS synthetic seismograms of the upper going and down going waves from the fracture in the homogeneous isotropic medium. In fact, it is impossible to record the down going wave (transmission) in the real seismic data. The homogeneous isotropic medium parameters are $v_p = 2300\text{m/s}$, $v_s = 1380\text{m/s}$, $\rho = 2.37\text{g/cm}^3$. $\mu = v_s^2\rho$, $\lambda=(v_p^2 - v_s^2)\rho$. In practical, it raises a question of the velocity once the background homogeneous isotropic medium is fractured to form azimuthal anisotropic medium (TI), the wave velocities in a spatial grid are part of changed from constant unique velocity into velocity weighted average by taking original and phase velocities, because there are not only background medium, but also fractured medium in one grid space after the medium fractured. Let's make an assumption that fracture's width is 2cm in a grid, according to the method of the volume weighted of each medium in a grid (Muir, et al., 1992), the various phase velocity only have one percent (2/200=1%) in a grid if there is a widely fracture aligned in the grid. So the velocity changing can be ignored in all the cases in this paper. Let us define values for Thomson's parameters to descript this azimuthal anisotropic medium: $\epsilon = 0.22$ it is the fractional difference between vertical and horizontal P velocity; $\gamma = 0.20$, it indicates the fractional difference between vertical and horizontal S velocity. Let's take the x-direction as horizontal and z-direction as the

vertical, then $z_N = (2\epsilon - h_f^2)/((1+h_f^2)(1-r)+2rh_f)$ and $z_t = 2\gamma/\mu$ are for horizontal fracture (z-normal to fracture) parameters tangential and normal compliances, respectively, where $r=\lambda^2/(\lambda+2\mu)^2$. Figure 3 shows the experimental geometries for three cases: horizontal, vertical and tilt fracture embedding in the homogeneous isotropic medium as well as velocities model.

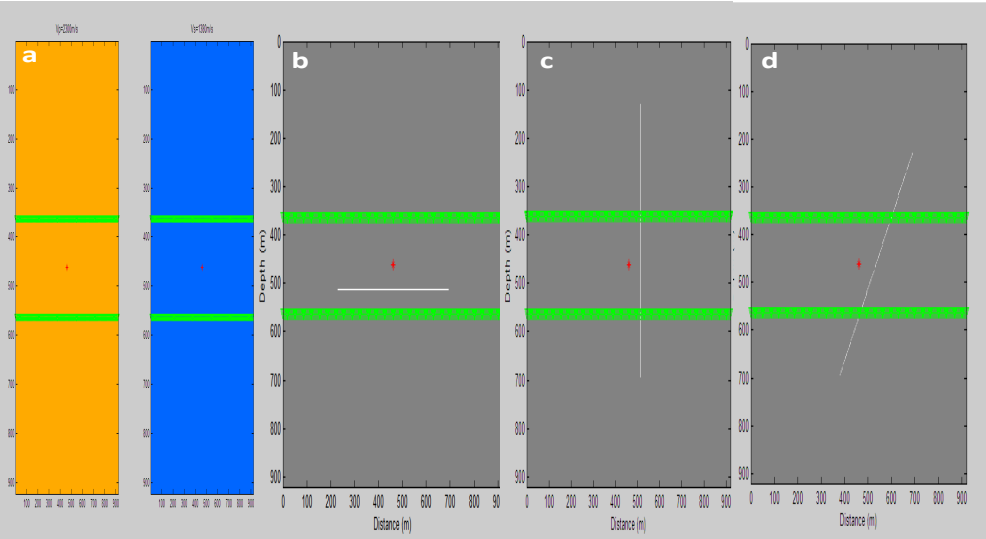

FIG. 3. The experimental geometries: the source is located at the central point of the model at grid 231x231. The receiver locations are horizontally above, below and vertical far from the source at 100m (grid∓50). The receiver interval is 2 grids. $\Delta x = \Delta z = 2m$. a) The velocity volumes. $v_p = 2300$m/s; $v_s = 1380$m/s; b) Case one: a horizontal fracture embedded in the homogeneous isotropic medium; c) Case two: a vertical fracture embedded in the homogeneous isotropic medium; d) Case three: a tilt fracture (60 degree) embedded in the homogeneous isotropic medium.

The finite difference scheme depends on the discrete grid variable (Lines, Slawinski and Bording, 1999). In order to avoid a problem of the FDs edge effects, it is helpful to extend spatial grids until the effective primary wave reflected from the fracture without the interfering coming from the four edges reflections. Thus the geometry has 461x461 spatial grids, its steps is $\Delta x=\Delta z=h=2.0$m and the time step is 0.0001ms. The source is located at the center of the model (grid: 231x231). The receive arrays are arranged horizontally above and below the source at a distance of 100m (∓50 grids). The Ricker wavelet was introduced as a source wavelet that is generated from an analog expression and using CREWES software. $\text{Ricker}(t)=(1-2\,\Pi^2 f^2 t^2)\exp(-\Pi^2 f^2 t^2)$ and then normalized. The normalization is a sinusoid of the dominant frequency that passes with unit amplitude (see CREWES software: wavenorm.m). The wavelet was multiplied with the value of positive and negative one as the source of force going up and down in the two directions (Figure 4). It has a specified frequency 40Hz in the range of normal seismic wave, the breadth is t=0.06ms, thus the wavelength $\lambda=57.5$m. It satisfied an equivalent effective medium assumption in long wavelength limit if the medium block is assumed to be the thickness H=5m.

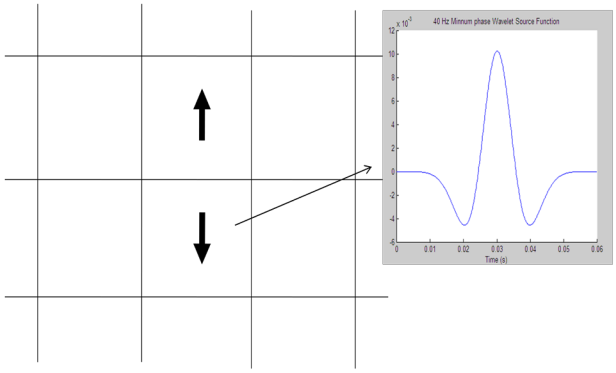

FIG. 4. A normalized Ricker wave is as a source wavelet.

For every case, it generated two kinds of the synthetic seismograms, one is for a fracture as a non-welded contact linear slip interface that is parallel to the grids, and the second is for the widely-spaced fractures and aligned to grids too. The examined case is for a horizontal fracture that is parallel to X axis and embedded in the homogeneous isotropic background medium. The fracture was horizontally inserted at 50m away below the source. The length of the fracture is 460m (grid: 115~345), see Figure 3(b). In this case, the direction of the wave propagation is normal to the fracture. The fracture tangential compliance (z_t) is in the xy-plane and normal to the direction of the wave propagation, whereas the fracture normal compliance (z_N) is in the yz-plane and parallel to the direction of the wave propagation. Figure (5a) illustrates x and z component seismograms and wave field for reflections (top: upper going wave) transmissions (bottom: down going wave). It is clearly shown that both PP and PS have been reflected from the horizontal fracture in the x and z components, in spite of no impedance contrast around the fracture. In the lower receivers array, they not only record the PP and PS direct arrival waves, but also PP and PS fracture reflection that leakage in. This simultaneously proves that there is no impedance contrast around the fracture.

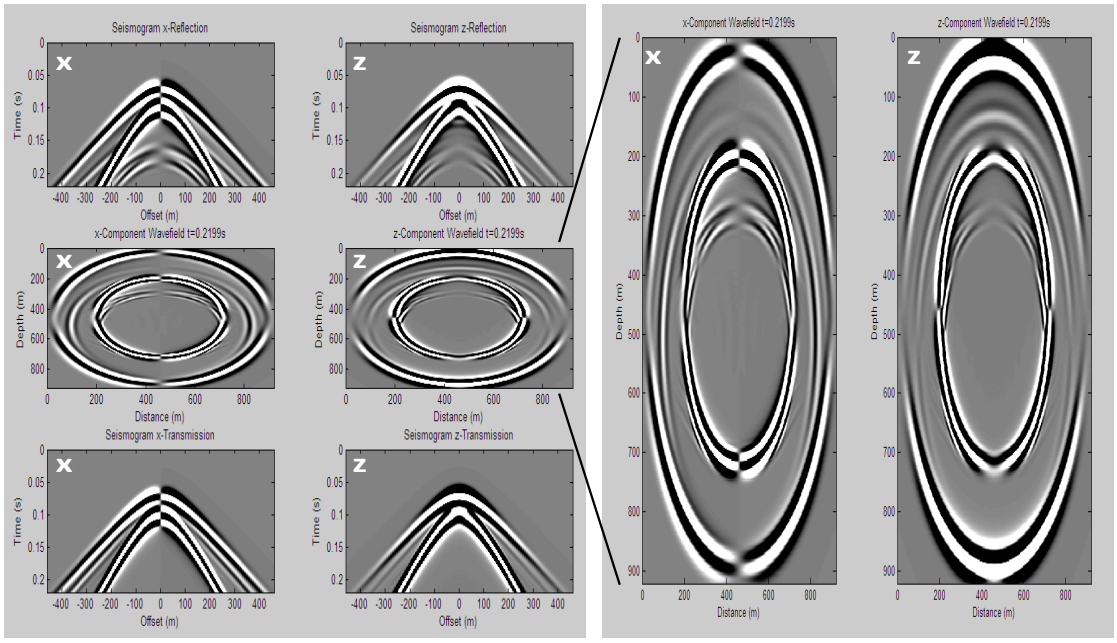

FIG. 5a. Synthetic seismograms and wave field for a horizontal fracture embedding in the homogeneous isotropic medium. The top left side is x and z components for upgoing wave from horizontal fracture. The bottom left side is x and z components for downgoing wave from the horizontal fracture. The middle part of the left side is x and z components wave field image. The right side is the zooming image of x and z components wave field.

In Figure (5b) , upper and down going wave seismograms have subtracted the PP and PS direct arrival wave, so it is easy to observe P-SV wave response from the horizontal fracture: PP and PS wave have been reflected from the horizontal fracture and the amplitudes are various with offset. The down going wave PS wave has stranger amplitudes than PP wave in the x and z components seismograms. Figure (5c) exhibits the difference between the fracture as a slip interface and the fracture with a width. It is assumed that the fracture relative thickness is h_f=2cm/5m=0.004 (the block layered medium has thickness 5m). It illustrates that the PP and PS up and down going waves are affected by the width of the fracture. The reason is that the width of the fracture only contribute to the normal compliance (z_n) of the fracture parameters in yz-plane, which means that the fracture normal compliance z_n various in the path of the wave propagation. Also, Figure (5c) exposes that the PS down going waves are more sensitive to width of the fracture than the upper going waves are. To explain, the direction of the PP wave polarization is normal to the fracture, thus the more PP wave have been reflected as upper going wave and less one have been transmitted as down going wave.

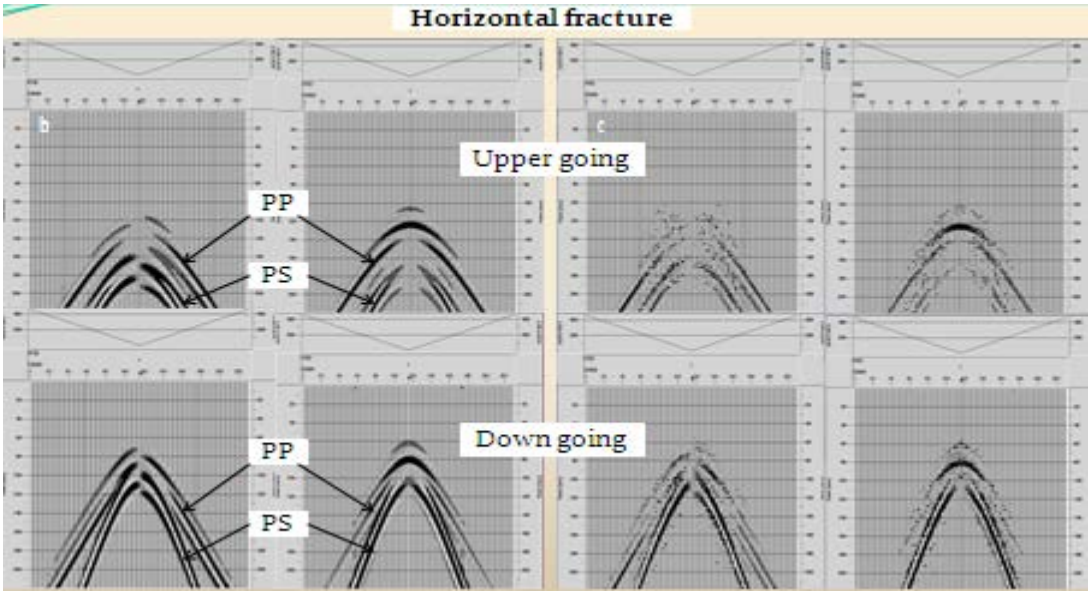

FIG. 5b. x and z components seismograms effects from the fracture as a non-welded contact linear slip interface. Figure 5c the different x and z components seismograms between a slip interface and a widely fracture.

A more realistic test for the vertical fracture is that to embed in the homogeneous isotropic background medium. In this case, the fracture was vertically inserted at 50m on the left away from the source. The length of the fracture is 560m (grid: 65~345), it has the same relationship of the source and receives as case one (Figure 3c). However, opposite to case one, the tangential compliance (z_t) of the fracture parameters are in yz-plane and normal to the x axis, whereas normal compliance (z_n) of the fracture parameters are in xy-plane and parallel to x axis. According to the geometry, the upper going wave have similar characters with down going wave. Figure 6a implies that the PP and PS direct waves are recorded in the upper and lower receivers in x and z component synthetic seismograms as well as the PP and PS reflections from vertical fracture. Because of the shear wave polarization is normal to the fracture, thus the more shear wave has been reflected than PP wave does (the top in Figure 6b).

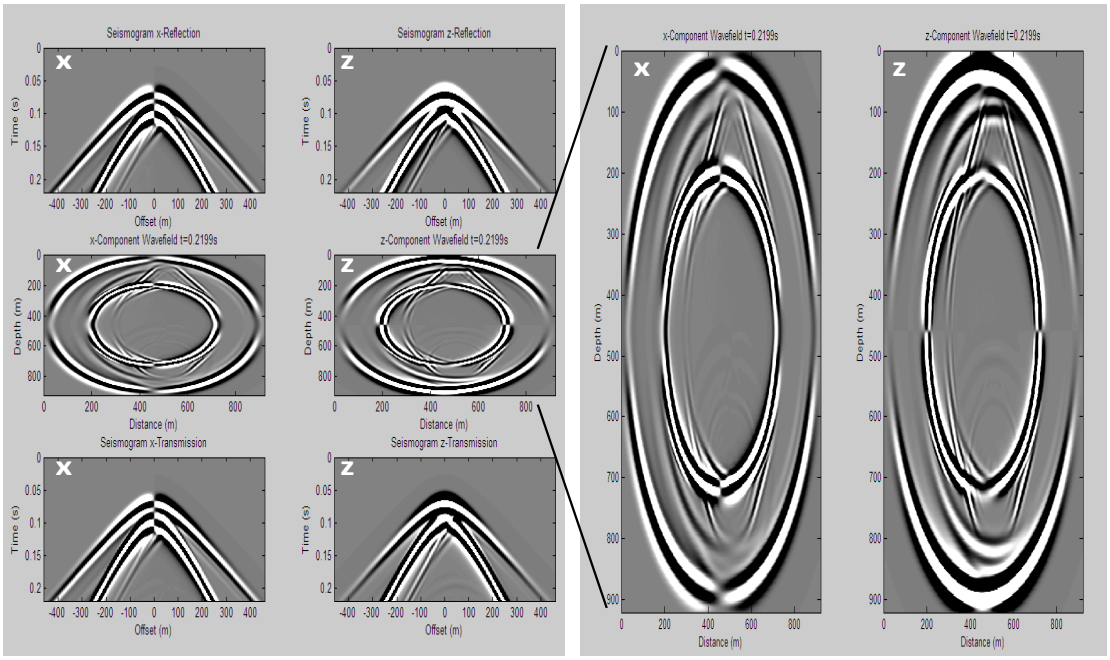

FIG. 6a. Synthetic seismograms and wave field for the vertical fracture embedded in the homogeneous isotropic medium. The top left side is x and z components seismograms for upgoing wave from vertical fracture. The bottom left side is x and z components seismograms for downgoing wave from the vertical fracture. The middle of the left side is x and z components wave field image. The right side is the zooming image of x and z components wave field.

Figure (6b) is seismograms recorded in upper and lower receives that subtracted the PP and PS direct arrival wave individually. Both x and z component seismograms shows that the PP amplitudes are various with the offsets, the near offset have stranger amplitude than the far offset has. Meanwhile, we observe a linear wave coming from the fracture interface. For comparison with the first case, it is explicit that the width of fracture is no longer sensitive to seismic wave, because the plane of the normal compliance of the fracture parameter is perpendicular to the direction of the wave propagation (figure 6c).

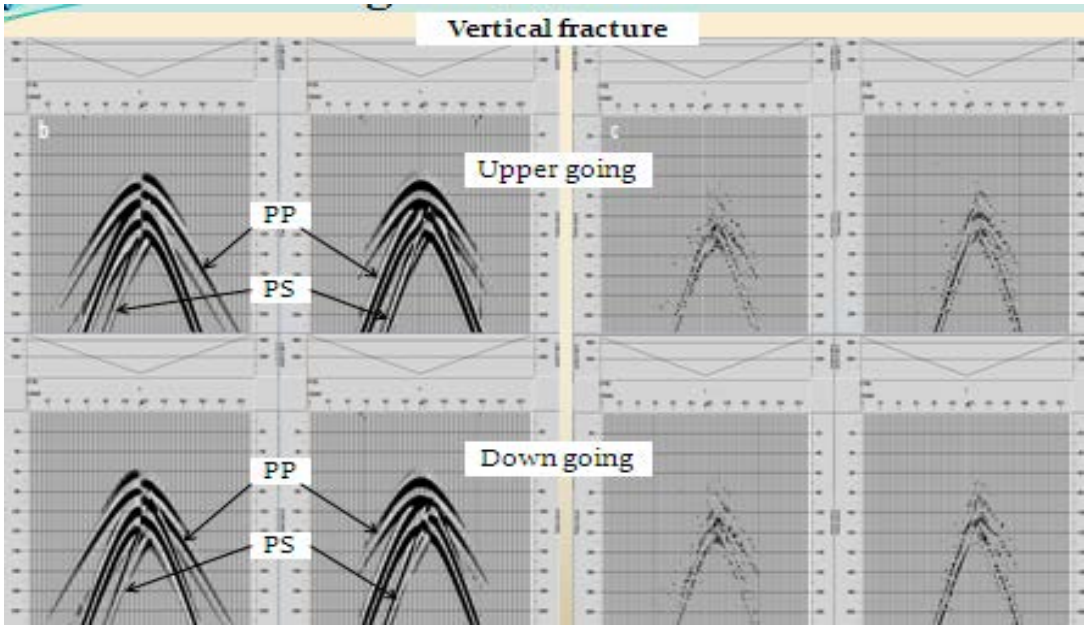

FIG. 6b. x and z components seismogram effects from the fracture as a non-welded contact linear slip interface. Figure 6c is the different x and z components seismograms between a slip interface and a widely fracture.

Figure 7a is synthetic seismograms and wave field for a tilt fracture embedding in the homogeneous isotropic medium. In this case, the fracture tilt was inserted in the background medium with 60 degree respect to horizontal axis. It has the same relationship of the source and receives as the case one and case two (Figure 3d). It is interesting that both normal compliance (z_n) and tangential compliance (z_t) of the fracture parameters are either in the yz-plane or in the xy-plane. The diagram7a demonstrates that the wave fields are more complicate than case one and case two since the dispersion is showing out. It means that seismic wave propagation goes through fracture rise scattering and amplitude changing.

Figure (7b) is synthetic seismogram that records from the upper and lower receives without the PP and PS direct wave. It illustrates that both PP and PS wave x and z components have recorded at the upper and lower receives. Figure (7c) shows that the fracture's width is not more sensitive to the wave propagation than case one (horizontal fracture), but it responds to the sensation more active than case two (vertical fracture). Note that the examination results in this case (tilt fracture) are taking in 2D domain and indistinguishable from the 3D domain or orthorhombic medium, therefore, the results from the tilt fracture are suitable to the case of the CHOPs

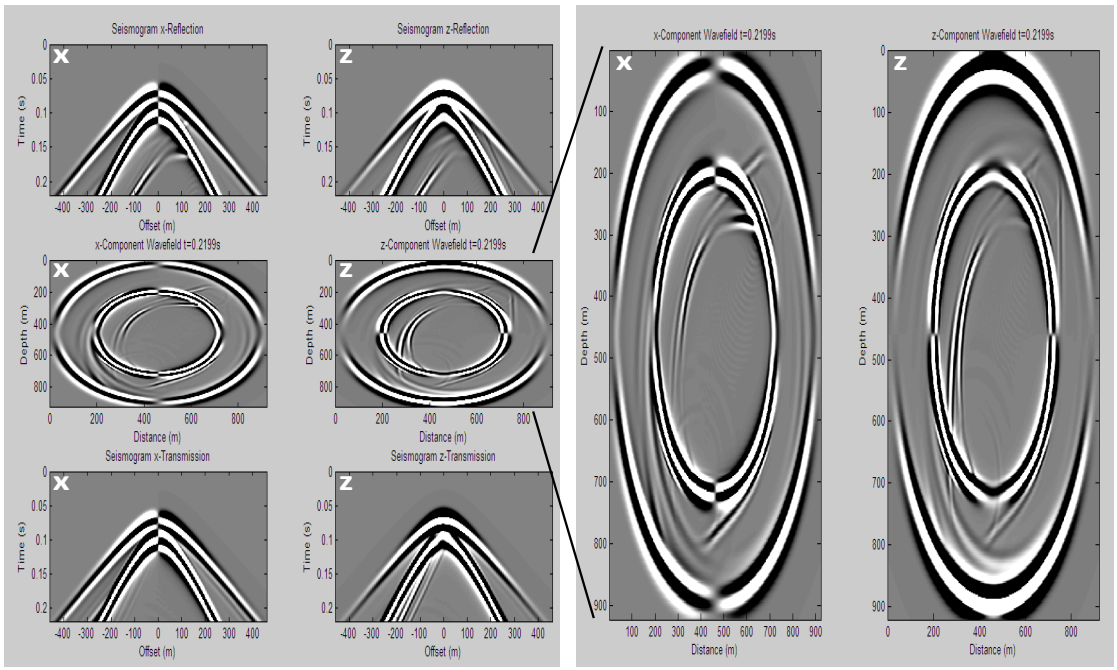

FIG. 7a. x and z component of the synthetic seismograms and wave field for tilt fracture embedding in the homogeneous isotropic medium. The top left side is x and z components seismograms for upgoing wave from tilt fracture. The bottom left side is x and z components seismograms for downgoing wave from the tilt fracture. The middle of the left side is x and z components wave field illustration. The right side is the zooming image of x and z components wave field.

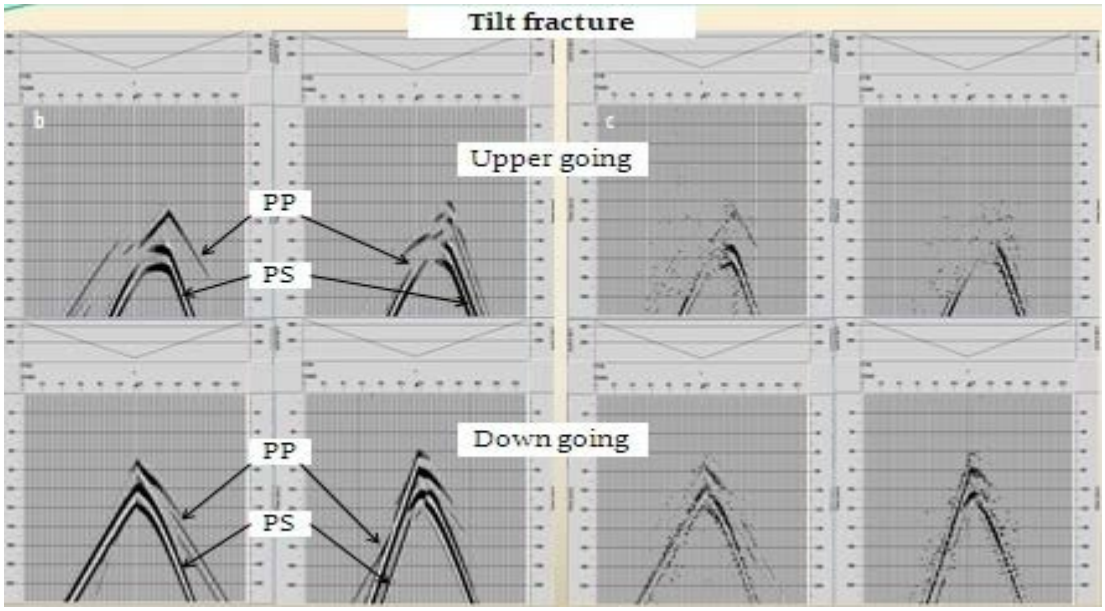

FIG. 7b. x and z components seismograms are affected by the fracture as a non-welded contact linear slip interface. Figure 7c indicates the difference of x and z components in seismograms between a slip interface and a widely fracture.

CONCLUSIONS

Note that there is no impedance contrast in the homogeneous isotropic medium, but there are still reflections that due to the displacement discontinuity across the fracture (equations 16a, 16b). Any kind of the fracture can be indicated by the seismic records. Since the fracture's width affects the normal compliance of the fracture parameter, the synthetic seismogram responses of the width of the fracture really depends on the relationship between the direction of the wave propagation and the plane of the fracture normal compliance.

ACKNOWLEDGMENTS

We would like to thank the sponsors of CREWES and CHORUS. Thanks Ge Zhan, Zaiming Jiang and Peng Cheng for discussions of the Matlab coding.

REFERENCES

Aki, K., and Richards, P. G., 1980, Quantitative seismology, theory and methods, volume 1: W H Freeman and Co, Cambridge Press, 144 – 154.

Backus, G. E., 1962, Long-wave anisotropy produced by horizontal layering: J. Geophys. Res., 66, 4,427-4,440, 1962.

Crampin, S., 1985, Evidence for aligned cracks in the Earth's crust: First Break, 3, no. 3, 12-15.

Coates, R.T., and Schoenberg, M., 1995, Finite-difference modeling of faults and fractures, Geophysics, 60, 1514-1526.

Hood, J. A., and Schoenberg, M., 1989, Estimation of vertical fracturing from measured elastic moduli: Journal of Geophysical Research, 94, 15,611–15,618.

Hsu, C. J., and Schoenberg, M., 1993, Elastic waves through a simulated fractured medium: Geophysics, 58, 964–977.

Korn, M., and Stockl, H., 1982, Reflection and Transmission of Love Channel Wave at Coal Seam, Discontinuities Computed with a Finite Difference Method. Journal of Geophysics, 50: 171-176

Lines, L.R., Daley, P.F., and Embleton, J.E., 2008, The resolution and detection of "subseismic" high-permeability zones in petroleum reservoirs: The Leading Edge May 2008 vol. 27 no. 5 664-669

Nichols, D., Muir. F., and Schoenberg, M., 1989, Elastic properties of rocks with multiple sets of fractures: 59th Ann. Internat. Mtg., Soc. Expl. Geophys.. Expanded Abstracts, 471474.

Pyrak-Nolte, L.J., L.R, Myer., and N.G.W. Cook., 1990b, Transmission of seismic wave across single natural fracture: J. Geophys. Res. 95. 8617-8638.

Raphael A. Slawinski., and Edward S. Krebes., 2000, Finite-difference modeling of SH-wave propagation in nonwelded contact media: Geophysics. vol. 67, No5

Ruger, Andreas., 1998, Variation of P-wave reflectivity with offset and azimuth in anisotropic media: Geophysics 63, 935.

Schoenberg, M., 1980, Elastic wave behavior across linear slip interfaces, J. Acoust. Soc. Am., 68, 1516-1521.

Schoenberg, M., and Douma, J., 1988, Elastic wave propagation in media with parallel fractures and aligned cracks: Geophysical Prospecting, 36, 571-590.

Schoenberg, M., and Muir, F., 1989, A calculus for finely layered anisotropic media: Geophysics, 54, 581–589.

Schoenberg, M., and Sayers, C.M., 1995, Seismic anisotropy of fractured rock: Geophysics, 60, 204-211.

Thomsen Leon., 1986, Weak elastic anisotropy: Geophysics. vol. 51, 1954-1966